



# Analyzing the generalization capabilities of a hybrid hydrological model for extrapolation to extreme events

Eduardo Acuña Espinoza<sup>1</sup>, Ralf Loritz<sup>1</sup>, Frederik Kratzert<sup>2</sup>, Daniel Klotz<sup>2,3</sup>, Martin Gauch<sup>4</sup>, Manuel Álvarez Chaves<sup>5</sup>, and Uwe Ehret<sup>1</sup>

<sup>1</sup>Institute of Water and Environment, Karlsruhe Institute of Technology (KIT), Karlsruhe, Germany

<sup>2</sup>Google Research, Vienna, Austria

<sup>3</sup>Helmholtz Centre for Environmental Research (UFZ), Leipzig, Germany

<sup>4</sup>Google Research, Zurich, Switzerland

<sup>5</sup>Stuttgart Center for Simulation Science, Statistical Model-Data Integration, University of Stuttgart, Stuttgart, Germany

**Correspondence:** Eduardo Acuña Espinoza (eduardo.espinoza@kit.edu)

Received: 10 July 2024 – Discussion started: 30 July 2024

Revised: 12 January 2025 – Accepted: 18 January 2025 – Published: 11 March 2025

**Abstract.** Data-driven techniques have shown the potential to outperform process-based models in rainfall–runoff simulation. Recently, hybrid models, which combine data-driven methods with process-based approaches, have been proposed to leverage the strengths of both methodologies, aiming to enhance simulation accuracy while maintaining a certain interpretability. Expanding the set of test cases to evaluate hybrid models under different conditions, we test their generalization capabilities for extreme hydrological events, comparing their performance against long short-term memory (LSTM) networks and process-based models. Our results indicate that hybrid models show performance similar to that of the LSTM network for most cases. However, hybrid models reported slightly lower errors in the most extreme cases and were able to produce higher peak discharges.

Recently, hybrid models that combine process-based models with data-driven approaches have been proposed (Reichstein et al., 2019; Shen et al., 2023). The idea behind hybrid models is that they integrate the strengths of both process-based and data-driven approaches to improve simulation accuracy while maintaining a notion of interpretability (Jiang et al., 2020; Höge et al., 2022). Among the various approaches available to combine these methodologies, the parameterization of process-based models using data-driven techniques has shown promising results (Tsai et al., 2021). One way to interpret this technique is that it involves integrating a neural network with a process-based model in an end-to-end pipeline, where the neural network handles the parameterization of the process-based model. Alternatively, this can be viewed as a neural network with a process-based head layer, which not only compresses the information into a target signal but has a certain structure that allows for the recovery of untrained variables. Kraft et al. (2022) applied this method, demonstrating that substituting poorly understood or challenging-to-parameterize processes with machine learning (ML) models can effectively reduce model biases and enhance local adaptivity. Similarly, Feng et al. (2022) and Acuña Espinoza et al. (2024) employed LSTM networks to estimate the parameters of process-based models, achieving state-of-the-art performance comparable with LSTMs and outperforming stand-alone conceptual models.

In a previous study, Acuña Espinoza et al. (2024) tested the performance and interpretability of hybrid models, with

## 1 Introduction

Data-driven techniques have demonstrated the potential to outperform process-based models in rainfall–runoff simulation (Kratzert et al., 2019; Lees et al., 2021; Feng et al., 2020). Moreover, Frame et al. (2022) addressed concerns about the generalization capability of data-driven methods for extrapolation to extreme events, demonstrating that long short-term memory (LSTM) networks (Hochreiter and Schmidhuber, 1997) outperformed process-based models in such scenarios.

the overall goal of looking at the advantages provided by adding a process-based head layer to a data-driven method. They show that hybrid models can achieve comparable performance with LSTM networks while maintaining a notion of interpretability. In this type of hybrid model, the interpretability arises from association. Specifically, the authors map the parameters and components of process-based models to predefined processes, domains, and states (e.g., baseflow, interflow, snow accumulation). While this approach does provide interpretability, it is important to clarify that this interpretability is, indeed, limited to associations and may lack rigorous physical principles, especially when one uses models such as the simple hydrological model (SHM) (Ehret et al., 2020) or the Hydrologiska Byråns Vattenbalansavdelning (HBV) (Bergström, 1992), which present significant simplifications of the underlying physical process. Moreover, Acuña Espinoza et al. (2024) also warn about the possibility that the data-driven section of the hybrid model compensates for structural deficiencies in the conceptual layer.

Building on this research line and expanding the set of test cases to evaluate hybrid models under different conditions, this study follows the procedure proposed by Frame et al. (2022) to investigate the ability of different models to predict out-of-sample conditions, focusing on their capability to generalize to extreme events. We compare the performance of hybrid models against both traditional process-based models and stand-alone data-driven models. We aim to determine which model demonstrates higher predictive accuracy, particularly in simulating extreme hydrological events. We thereby address the following two research questions:

- How does a hybrid model compare to a process-based model and a stand-alone data-driven model in the simulation of extreme hydrological events?
- Does hybrid modeling offer a higher performance than stand-alone data-driven approaches?

To achieve this objective, we have structured this article as follows: Sect. 2 describes the training data–test data split and gives an overview of the different models. In Sect. 3, we compare the results of various tests that assess the generalization capabilities of data-driven, hybrid, and conceptual models. Lastly, Sect. 4 summarizes the key findings of the experiments and presents the conclusions of the study.

## 2 Data and methods

Donoho (2017) emphasize the importance of community benchmarks in driving model improvement. In the hydrological community, this practice has also been suggested to enable a fair comparison between new and existing methods (Shen et al., 2018; Nearing et al., 2021; Kratzert et al., 2024). Consequently, we built our experiments considering two existing studies. First, we used the procedure proposed

by Frame et al. (2022) to evaluate the generalization capability of different models (see Sect. 2.1). In accordance with this study, the experiments were conducted using the CAMELS-US dataset (Addor et al., 2017; Newman et al., 2015) in the same subset of 531 basins. Second, we used the hybrid model architecture  $\delta_n(\gamma^t, \beta^t)$ , further explained in Sect. 2.2.2, as proposed by Feng et al. (2022). This architecture demonstrated competitive performance compared to LSTM networks in their original experiments, which also used the CAMELS-US dataset.

### 2.1 Data handling: training–test split

To produce an out-of-sample test dataset and to evaluate the generalization capability of the different models for extreme-streamflow events, we split the training and test sets by years based on the return period of the maximum annual discharge event. Closely following the procedure recommended by Bulletin 17C (England et al., 2019), we fitted a Pearson III distribution to the annual maxima series of each basin, which we extracted from the observed CAMELS-US discharge records. We then calculated the magnitude of the discharge associated with different probabilities of exceedance. Using the discharge associated with the 5-year return period as a threshold, we classified the water years (here, a water year is defined as the period of time between 1 October and 30 September of the following year) into training or test sets. Figure 1a shows an example of the training–test split for basin no. 01054200 in the northeast of the United States (US). The water years which contained only discharge records smaller than the associated 5-year threshold were used for training, while cases in which this threshold was exceeded were used for testing. It is important to note that there was a 365 d buffer between each training and testing period. The value of 365 d corresponds to the sequence length used by the LSTM model, and the buffer period avoids the leaking of test information during training. The results of the frequency analysis and the training data–test data split for each basin can be found in Acuña Espinoza (2024). The original dataset contained 531 basins, each with 34 years of data (from 1980 to 2014), for a total of 18 054 years of data. After the data split process, 9489 years were used for training, 3429 years were used for testing, and 5136 years were buffers. Excluding the buffer data, 73 % of the data were used for training and 27 % were for testing. This distribution is consistent with the 80 %–20 % theoretical split associated with the 5-year return period.

It should be noted that the results from the training data–test data split differed from the ones proposed by Frame et al. (2022). In their study, the frequency analysis was done with instantaneous peak flow observations taken from the USGS NWIS (US Geological Survey, 2016), and a maximum cap of 13 water years was used to train each basin. Instead, we used the observed daily data from the CAMELS-US dataset and did not impose restrictions on the maximum number of

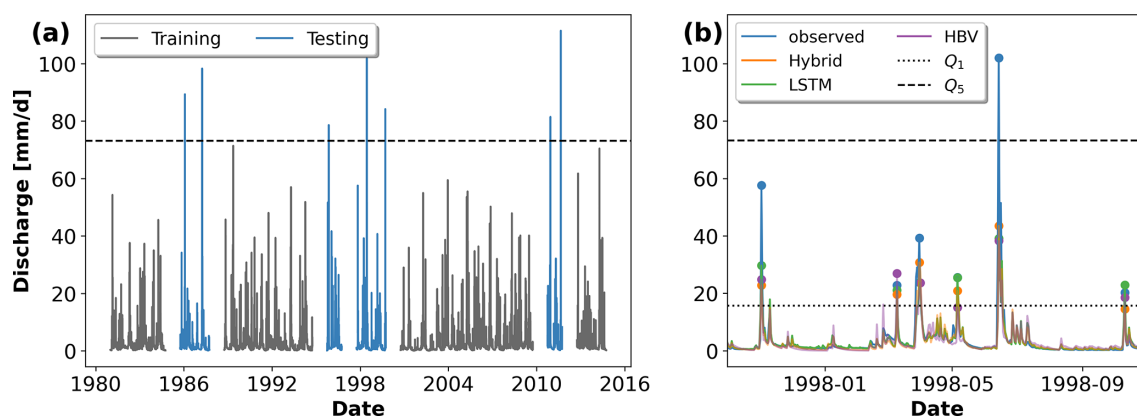


**Figure 1.** (a) Observed discharge ( $\text{mm d}^{-1}$ ) from 1984 to 2016 for catchment ID no. 01054200. Gray lines represent training data, including discharge below the 5-year return period threshold, marked by the dashed line ( $Q_5$ ). Blue lines indicate test data for discharge exceeding this threshold. This training–test split, based on discharge exceedance probability, is designed to assess model performance under extreme hydrological conditions. (b) Example of peak identification for basin no. 01054200 for 1 year within the test period.  $Q_1$  represent the 1-year return period threshold, which was used to identify peak events.  $Q_5$  represent the 5-year return period threshold, which was used for the training data–test data split.

training years. We would also like to re-emphasize that training the model exclusively on water years containing events smaller than a 5-year return period and testing it on water years with events larger than a 5-year return period was meant as a form of stress test to get a sense of the model behavior with regard to extreme-streamflow events. In practical applications, one would not choose to use this type of setup, but one should use all available information about this kind of event for model training.

## 2.2 Data-driven, hybrid, and conceptual models

The experiments in this study were conducted using three models: a stand-alone LSTM, the HBV model as a stand-alone conceptual model, and a hybrid approach. Both the LSTM and the hybrid model were trained using the NeuralHydrology (NH) package (Kratzert et al., 2022), while the optimization of the stand-alone conceptual model used the SPOTPY library (Houska et al., 2015). Consistently with previous studies, the LSTM and hybrid models were trained regionally using the information from all 531 basins at the same time, while the stand-alone conceptual model was trained basin-wise (locally). In other words, in this study, we compare the model results of an LSTM network, a hybrid model, and 531 individually trained conceptual models.

### 2.2.1 LSTM

The hyper-parameters for the stand-alone LSTM were taken from Frame et al. (2022). We used a single-layer LSTM with 128 hidden states, a sequence length of 365 d, a batch size of 256, and a dropout rate of 0.4. The optimization was done using the Adam algorithm (Kingma and Ba, 2014). An initial learning rate of  $10^{-3}$  was selected, which was de-

creased to  $5 \times 10^{-4}$  and  $10^{-4}$  after 10 and 20 epochs, respectively. The basin-averaged Nash–Sutcliffe efficiency (NSE) loss function proposed by Kratzert et al. (2019) was used for the optimization. In a slight deviation from Frame et al. (2022), we trained our model for 20 epochs instead of 30. We trained our models using five dynamic inputs from the Daymet forcing – precipitation ( $\text{mm d}^{-1}$ ), average shortwave radiation ( $\text{W m}^{-2}$ ), maximum temperature ( $^{\circ}\text{C}$ ), minimum temperature ( $^{\circ}\text{C}$ ), and vapor pressure (Pa) – and 27 static attributes, listed in Table A1 in the Appendix of Kratzert et al. (2019), describing the climatic, topographic, vegetation, and soil characteristics of the different basins.

We used an ensemble of five LSTM networks to produce the final simulated discharge. In other words, we trained five individual LSTM models with the architecture described above but initialized each one using a different random seed. After training, we ran each model, individually, to retrieve the simulated discharges, and we took the median value as the final discharge signal, which we used in the analysis. Using an ensemble of LSTM networks allows us to produce more robust results (Kratzert et al., 2019; Lees et al., 2021; Gauch et al., 2021) and reduces the effects associated with the random initialization of the models.

### 2.2.2 Hybrid model: LSTM and HBV

For the hybrid model architecture, we used the  $\delta_n(\gamma^t, \beta^t)$  model proposed by Feng et al. (2022). In this architecture, an ensemble of 16 HBV models acting in parallel was parameterized by a single LSTM network. Each of the 16 ensemble members contained an HBV model with four buckets, whose flows were controlled by 11 static and 2 time-varying parameters. The discharge of the ensemble was calculated as the mean discharge of the 16 members. Moreover, to produce

the final outflow, the ensemble discharge was routed using a two-parameter unit hydrograph. In total, the LSTM produced 210 parameters (16 ensemble members, each with 13 HBV parameters and 2 routing parameters) which were used to control the ensemble of conceptual models, as well as the routing scheme. The model was trained end to end. Figure A1 in Appendix A shows a scheme of the hybrid model structure.

During training, each batch contained 256 samples, each with a sequence of 730 d. The first 365 d were used as a warmup period to stabilize the internal states (buckets) of the HBV and to reduce the effect of the initial conditions. These 365 values did not contribute to the loss function. The remaining 365 time steps were used to calculate the loss, back-propagate the gradients, and update the model's weights and biases. Further details on the model implementation can be found in the `hybrid_extrapolation_seed#.yaml` files of the Supplement. To validate our pipeline, we benchmarked our hybrid model implementation using the experiments proposed by Feng et al. (2022). These results are shown in Appendix A, where we show a similar performance between our implementation and their results. Only after validating our pipeline did we run the extrapolation experiments.

### 2.2.3 Stand-alone conceptual model: HBV

To have a full comparison of the model spectrum, we also included a stand-alone conceptual model. We used a single HBV model plus a unit hydrograph routing routine, resulting in a model with 14 calibration parameters (12 from the HBV and 2 from the routing). Note that this HBV instance has one less parameter (12 instead of 13) than the version used in the hybrid model. This one-parameter difference is to maintain consistency with Feng et al. (2022), where the authors used the 13-parameter HBV only when dynamic parameterization was included and the 12-parameter model for the static version. Similarly to Acuña Espinoza et al. (2024), the stand-alone conceptual models were trained basin-wise using shuffled complex evolution (SCE-UA) (Duan et al., 1994) and Differential Evolution Adaptive Metropolis (DREAM) (Vrugt, 2016), both implemented in the SPOTPY library (Houska et al., 2015). We then selected, for each basin, the calibration parameters that yielded better results.

### 2.3 Performance metrics

To evaluate the overall performance of the model, we used the Nash–Sutcliffe efficiency (NSE) (Nash and Sutcliffe, 1970). However, the main objective of this study is to evaluate the ability of the models to predict high-flow scenarios. Therefore, the majority of the analyses were done using only peak flows.

Given the amount of data comprised in the test period (3429 years over the 531 basins), the peak identification was done automatically. For this task, we used the `find_peaks`

function of the signal module in the SciPy library (Virtanen et al., 2020), defining a 7 d window as the criterion for independent events. Moreover, we selected only the peaks above the 1-year return period threshold to have a better representation of high-flow scenarios. After we identified the peaks in the observed discharge series, we extracted the associated values from the simulated series of the different models. Figure 1b exemplifies this process for basin no. 01054200 for 1 year within the test period, where each dot represents an identified peak. Once the peaks were identified, we calculated the absolute percentage error (APE) as a metric for model performance:

$$\text{APE} = \frac{|y_{\text{obs}} - y_{\text{sim}}|}{y_{\text{obs}}}, \quad (1)$$

where  $y_{\text{obs}}$  and  $y_{\text{sim}}$  are the observed and simulated discharge, respectively.

## 3 Results and discussion

After training the models, we performed multiple analyses to evaluate their generalization capabilities to extreme events. The results of these analyses are presented in this section. All the results discussed here are for the test period.

### 3.1 Model performance comparison for whole test period

Figure 2 shows the cumulative distribution functions (CDFs) for the NSE reported for each model over the whole test period. We can see that the LSTM outperforms the hybrid model, with median NSE values of 0.75 and 0.71, respectively. Moreover, both models outperform the stand-alone HBV model, which has a median NSE value of 0.64. The result that both the LSTM and the hybrid model outperform the stand-alone HBV is not surprising, and similar results have been reported in the literature (Kratzert et al., 2019; Lees et al., 2021; Loritz et al., 2024; Feng et al., 2022; Acuña Espinoza et al., 2024). This can be attributed to the fact that conceptual models present a relatively simple structure that, in a lot of cases, oversimplifies the actual physical processes. For example, the HBV model assumes that all flows have a linear relationship with the storage; that the storage and/or discharge rate does not change over time; and that snow melting is a linear process, proportional to the difference between a threshold temperature and the air temperature. Both the LSTM and hybrid model have more flexible frameworks that allow them to increase their performance. Moreover, we show that, even with a different training–test split compared to the usual temporally contiguous subsets, our results are consistent with the ones reported by Feng et al. (2022) and Acuña Espinoza et al. (2024), where the same model ranking was observed.

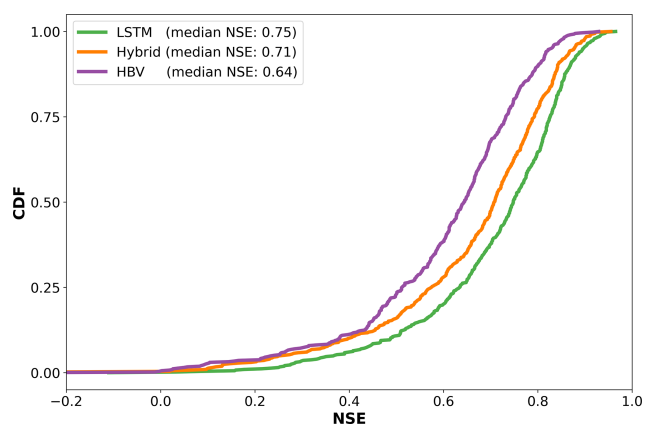


**Figure 2.** Cumulative density function (CDF) of the Nash–Sutcliffe efficiency (NSE) for the different models, generated using 531 basins of the CAMELS-US dataset. The NSE was calculated over the whole test period of each basin.

### 3.2 Model performance comparison for peak flows

The metrics shown in Fig. 2 were calculated using the whole test period. Consequently, they summarize the overall performance of the three models. However, the main objective of this study is to evaluate the ability of the models to predict high-flow scenarios. For this, we used the APE metric, which we calculated following the procedure described in Sect. 2.3. Figure 3a presents, for each model, the distribution of the APE for all of the peak flows. This figure shows a similar distribution for the three models, with the LSTM presenting a slightly lower median error than the hybrid and stand-alone HBV. Lower values are better for the APE metric. The finding that LSTMs outperform process-based models aligns with Frame et al. (2022) and helps to challenge the notion that data-driven methods are less capable of extrapolation (Reichstein et al., 2019; Slater et al., 2023). In the case of the hybrid model, although the LSTM exhibits a slightly lower median error, the error distributions of both models are similar. Therefore, we do not find strong evidence suggesting that one architecture is significantly better than the other in this scenario, leaving it to the reader's discretion to choose the model that best suits their needs.

### 3.3 Model performance comparison for out-of-sample peak flows

Figure 3a allowed us to evaluate the performance of the models only in peak discharges. However, this still did not give us a performance metric for values exclusively outside of the training range. More specifically, the results presented in Fig. 3a evaluated the error in 17 580 observed events. Considering the fact that the test period contained 3429 years, we got an average of five peaks per year. However, as shown in Fig. 1b, these peaks were not necessarily larger than the 5-year return period thresholds used during training. Figure 3b

shows the same error metric but classifies the peaks based on their return period. The four categories to the right of the vertical dashed line present the errors associated with discharges beyond the 5-year return period threshold, giving a strict evaluation of the generalization capabilities of the models. We can see that the LSTM outperformed the hybrid and HBV models slightly in the 1–5-year and 5–25-year return periods. In the remaining three intervals, the performance of the LSTM and hybrid are comparable, with the HBV also showing similar behavior for the last one. Figure B1 in Appendix B shows the variation in the APE due to five random initializations of the models. We can see that, in the last three categories, the LSTM performed better in three cases, the hybrid performed better in seven cases, and they both reported the same median value in four cases. Moreover, the differences in the median values between the LSTM and the hybrid model are smaller than the metric variation due to the random initialization, supporting our hypothesis that, for higher return periods, all models perform similarly.

In most cases, the errors increased for higher return periods. This was expected as models were trying to generalize to flows farther away from their training range. On the other hand, the peaks of the return period of 100+ years presented similar or slightly lower errors than the ones in the 50–100-year category. At this point, the reported errors were close to 60 %, which indicated that no model could satisfactorily reproduce the observed peaks. Moreover, because of the characteristic of the metric (see Eq. 1), the error was scaled by the magnitude of the observation, which would explain why the 50–100 and 100+ presented similar errors.

### 3.4 Spatial analysis of model performance

To further understand the capacity of the different models, we evaluated their performance in space, examining how predictive accuracy varies across regions and identifying differences between the models. As shown in Fig. C1 in Appendix C, all models exhibited lower performance in the basins located in the Great Plains (center) and in the southwest of the US. This pattern, previously documented in the scientific literature for both data-driven methods (Gauch et al., 2021) and process-based models (Newman et al., 2015), is also observed in the hybrid architecture, as demonstrated here. Martinez and Gupta (2010) identified the aridity ( $PET/P$ ) and runoff ratio ( $Q/P$ ) as good predictors of model performance. The comparison between Figs. C1 and C3 supports this hypothesis, revealing an association between lower performance and regions characterized by high aridity and low runoff ratios.

Given the shared behavior between the models, and in line with the objective of this comparison study, we further evaluate the differences in their performance. Figure 4 shows the difference between the hybrid and the LSTM model, calculated as  $APE_{\text{hybrid}} - APE_{\text{LSTM}}$ . Consequently, negative (blue) values indicate that the hybrid model performed better (i.e.,

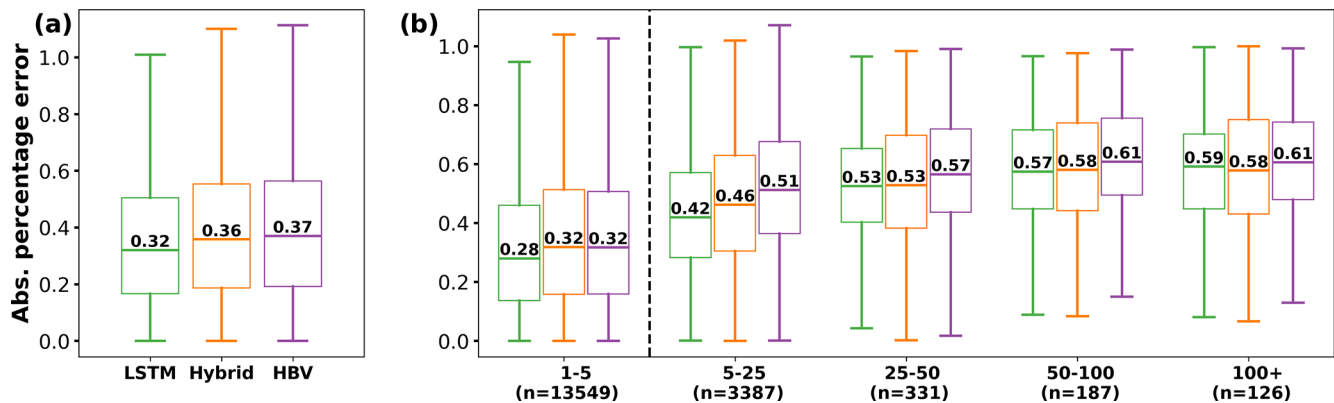


**Figure 3.** (a) Absolute percentage error (APE) between the observed peak discharge and the associated simulation value for the different models. The results show the error distribution from all 531 basins, calculated only for the peak flows of their test period (total of 17 580 values). (b) APE classified by the return period of the observed peaks. The four categories to the right of the vertical dashed line present the errors associated with observed discharge above the 5-year return period threshold, evaluating the out-of-sample capabilities of the models. The  $n$  value below each category indicates the amount of data used to produce the boxplot.

presented lower error), while positive (red) values favor the LSTM.

The first spatial tendency that we can notice is that, along the central part of the US, the LSTM tends to perform better. As previously discussed, this area is characterized by arid basins. In arid basins, surface runoff can be associated with high-intensity events over a short time period. Moreover, the HBV model generates runoff under the assumption that the discharge is a function of the basin storage and lacks a direct channel to transform precipitation into surface runoff (e.g., the water always routes through a linear reservoir). This assumption might not hold for the runoff-generating process in arid basins. Considering the fact that the hybrid model is regularized by an HBV layer, this structural deficiency would explain why the LSTM outperforms the hybrid model in this area.

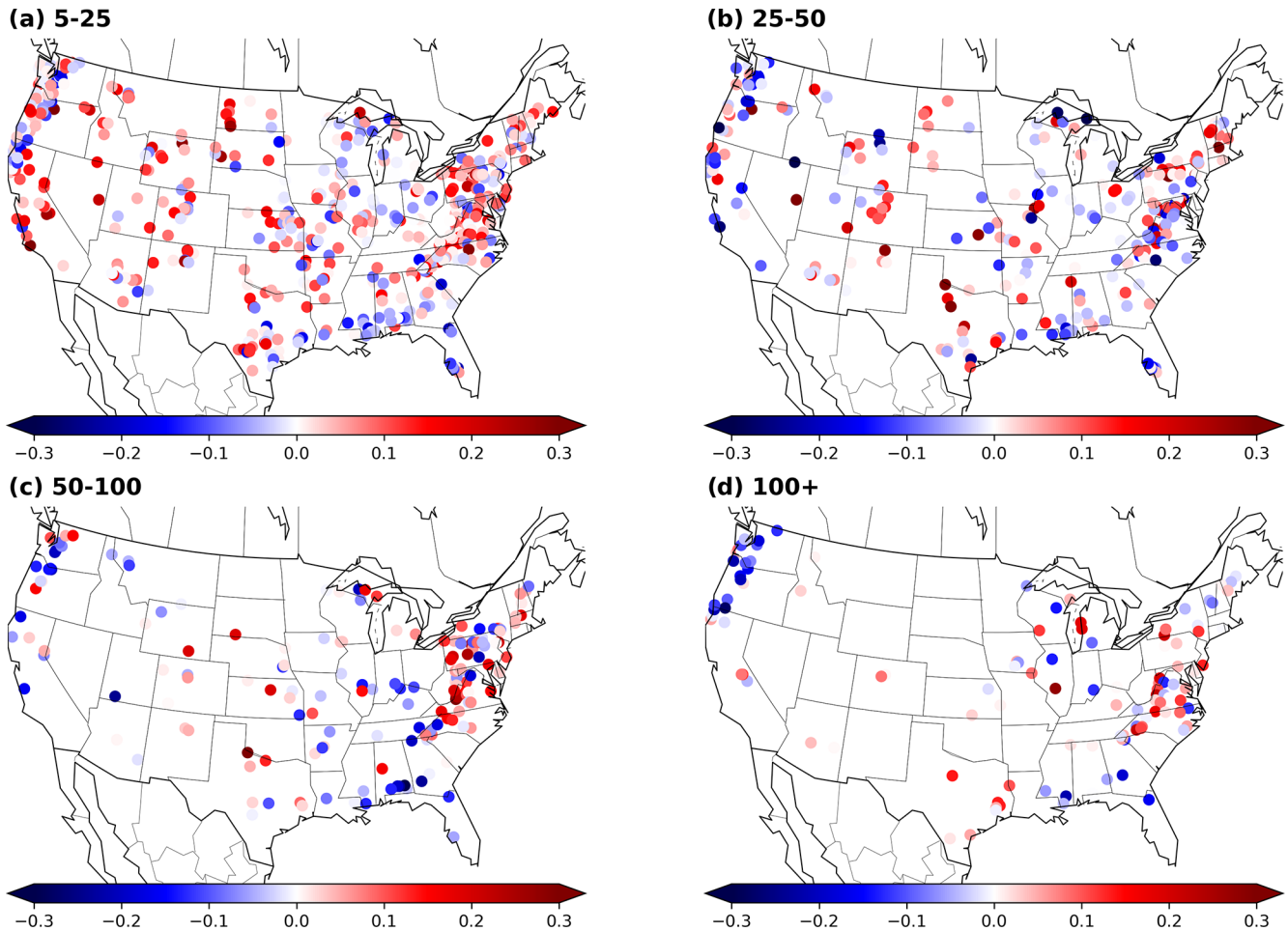
The second spatial tendency that we can observe is that, for the map of the return period of 100+ years, there is a cluster over the Pacific Northwest in which the hybrid model outperforms the LSTM. These basins are characterized by high precipitation values (see Fig. C3c) and high discharges. This is a challenge for the LSTM architecture due to saturation problems, which will be explained in detail in the next section.

Figure C1 further presents the differences between the HBV and LSTM models, as well as between the hybrid model and HBV. In the first case, the LSTM outperforms the HBV in most cases, with the same exception of the northwestern coast for the return period of 100+ years. In the second case, the hybrid model presents an overall better performance.

### 3.5 Saturation analysis: behavior of the models during extreme-flow scenarios

The saturation problem in LSTM models with a single linear head layer (as described by Kratzert et al., 2024) arises due to the inherent limitations of the model architecture, resulting in a theoretical prediction limit (see Eq. B2 of Kratzert et al., 2024). In other words, independently of the input series, the associated prediction cannot go above the theoretical limit. This limit is a function of the weights and biases of the head linear layer and varies for each trained model instance. From our experiments, where the model is trained only on discharge values below a 5-year return period, we observed that the maximum value predicted by the LSTM was  $78.9 \text{ mm d}^{-1}$ , which is close to the calculated theoretical prediction limit of  $83.9 \text{ mm d}^{-1}$ . This saturation limit could explain the LSTM's low performance for the cluster of basins in the Pacific Northwest of the US for the return period of 100+ years. Out of the 10 basins with the highest errors within this cluster, 7 of them presented discharges for the return period of 100+ years that were above the saturation limit of the LSTM. Therefore, independently of the forcing series, the model was not able to reach such values. Figure 5a shows an example in which this saturation problem is particularly pronounced. On the other hand, both the hybrid and the stand-alone HBV model do not have such a theoretical limit. The conceptual model architecture is defined with an unlimited capacity in the buckets, and, due to mass conservation, the water received by the models after evapotranspiration and other abstractions must be accounted for within the system.

The theoretical prediction limit in the LSTM is a function of the weights and biases of the head layer, which are a result of the training process. In our experiment, we artificially restricted the training data to discharges smaller than



**Figure 4.** Spatial visualization of the difference between the absolute percentage error (APE) for the hybrid and LSTM models. Each point corresponds to one basin. The four maps are associated with the different return periods. The color scale indicates the difference between the median APE for the different models. The difference is calculated as  $APE_{\text{hybrid}} - APE_{\text{LSTM}}$ ; therefore, negative (blue) values indicate that the hybrid model performs better, and positive (red) values indicate that the LSTM performs better.

the 5-year return period thresholds, reducing the support of the data space the model was fitted to. Consequently, this setup directly intensified the saturation problem. In practical applications where the model is trained on all available data, the saturation issue would tend to decrease in relevance. Moreover, it would only affect the few gauges in which the extreme discharges are above the saturation limit. However, a theoretical saturation limit remains, which is an undesirable property in a hydrological model, especially in cases where we are designing infrastructure for extreme events outside of any training data (e.g., 1000-year flood). Further research should be invested in overcoming this problem.

Apart from the statistical artifacts introduced by our selection procedure, we found two potential issues that might lead to the peak underestimation of the hybrid models. Figure 6 shows the precipitation and observed discharge, together with the accumulated value and the simulated discharge series, for four of the largest events in the dataset.

For basin nos. 08178880 and 08200000, the accumulated precipitation of the event is similar to or larger than the accumulated discharge; however, the simulated series strongly underestimates the discharge. This behavior can arise due to structural limitations in the hydrological model. For example, given the lack of a fast response channel, a high precipitation pulse can be divided and routed through several linear reservoirs, attenuating the respective discharge peak. This effect could have been strengthened by our training–test split, given that the optimization parameters, which control the interaction between the buckets, were learned for certain conditions, which were inadequate for other out-of-sample hydrological events.

In this regard, the hybrid model presents a theoretical advantage over the HBV model through the possibility of dynamic parameterization that adapts the model behavior to current conditions. The  $\delta_n(\gamma^t, \beta^t)$  hybrid model uses a dynamic  $\beta$  coefficient to control the recharge rate at which pre-

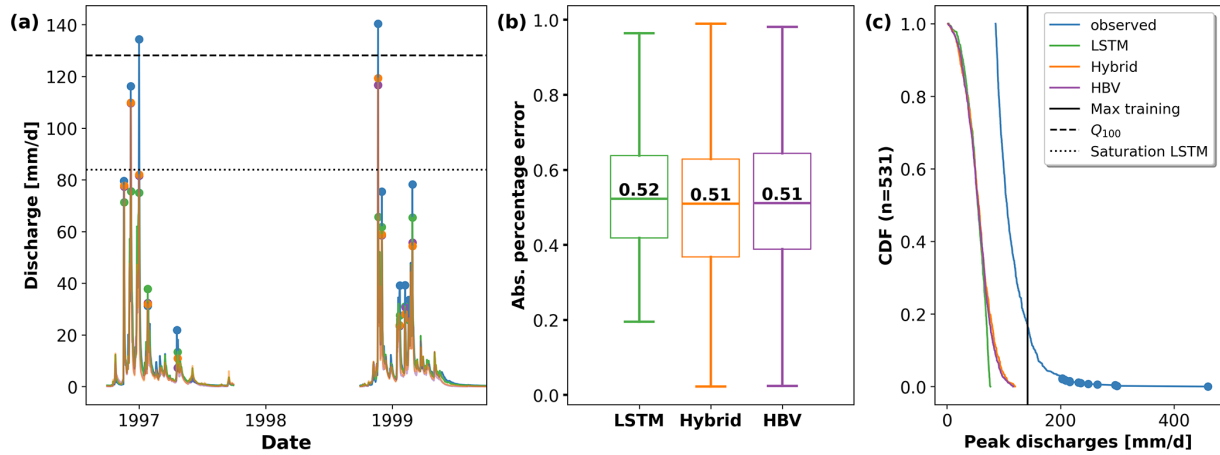


**Figure 5.** (a) Observed and simulated discharges for 2 years of the testing period for basin no. 11532500. The dashed and dotted lines indicate the 100-year return period discharge and the theoretical saturation limit of the LSTM model, respectively. (b) Absolute percentage error (APE) of the 531 highest discharges for the different models. (c) Cumulative density function (CDF) of the 531 observed highest discharge values across all basins and their respective simulated values. The blue dots help visualize the fact that less than 3 % of the events have values between 200 and 400 mm d<sup>-1</sup>.

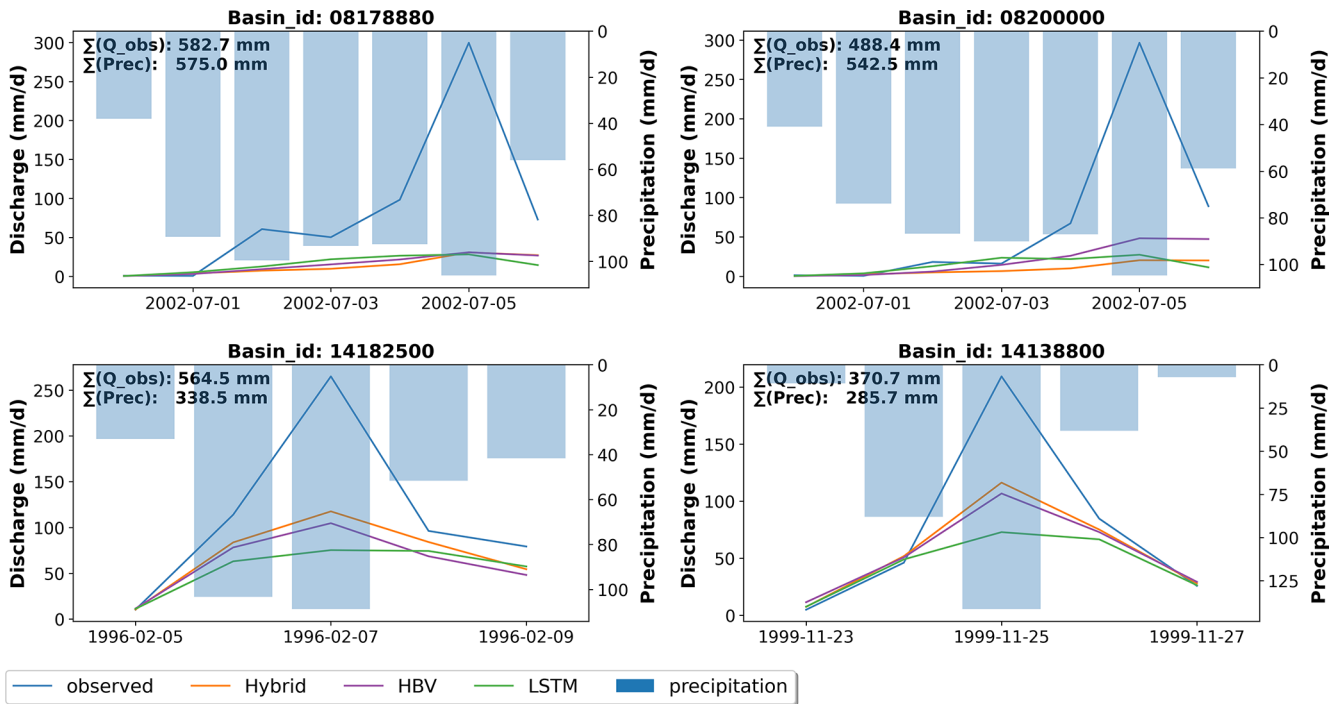


**Figure 6.** Example of four of the most extreme events presented in the dataset. The subplots show the precipitation series and the observed and simulated hydrographs.  $\Sigma Q_{obs}$  and  $\Sigma Prec$  indicate the cumulative sum of the discharge and precipitation series. Basin nos. 08178880 and 08200000 have similar precipitation and discharge volumes, while basin nos. 14182500 and 14138800 have a precipitation volume that is smaller than the discharge volume.

precipitation was transferred to the other buckets. However, as discussed in the previous paragraph and as shown in Fig. D1, during high-intensity events,  $\beta$  reached the limits of its predefined interval, which limited the model in further adapting its behavior.

The second issue that we found is a possible bias in the input data. For basin nos. 14182500 and 14138800, the accumulated precipitation is smaller than the accumulated discharge, which would explain the underestimation of the simulated values. Westerberg and McMillan (2015) indicate that bias in precipitation measurements can be caused by



point uncertainty, interpolation uncertainty, and equipment malfunction. Moreover, Bárdossy and Anwar (2023) indicate that catchment-averaged precipitation values present a higher bias during extreme events. This bias poses a challenge for the HBV and hybrid models, which rely on a mass-conservative structure. Without sufficient water input into the system, the model inherently cannot replicate the observed discharges.

An alternative hypothesis to precipitation bias is that the high discharges are caused by snowmelt or glacier melt. In this case, the accumulated precipitation during the event can be smaller than the accumulated discharge since part of the discharge would be caused by melting water that entered the system weeks or months before. Both basins are located in the state of Oregon (northwestern USA), and, accounting for the dates of both events, there is a possibility for snowmelt-induced discharge. Nevertheless, the snow module of HBV does not reproduce this behavior, which would point towards a structural deficiency in the model.

### 3.6 Limitations and uncertainties

In this study, we focus our results and analysis on model performance as we tackled our research questions from a practitioner's point of view. However, it should be noted that other criteria, such as model interpretability, also play an important role in an integral model evaluation as these allow us to assess whether the generated results align with expected domain-specific behaviors. Appendix D briefly discusses the temporal variation in the dynamic parameters for the hybrid model in this context. We further refer to studies such as those of Acuña Espinoza et al. (2024), Kraft et al. (2022), Höge et al. (2022), and Feng et al. (2022) for a deeper analysis of model interpretability for hybrid models.

Following the procedure proposed by Frame et al. (2022), we split the training and test periods by years based on the return period of the maximum annual discharge. Both periods used information from the previously selected 531 basins. In future work, one could use different subsets of basins during training and testing to further compare the models based on an ungauged basin scenario and evaluate their spatial generalization capability.

The comparison presented here was done using the hybrid architecture proposed by Feng et al. (2022). This architecture was chosen because it gave a competitive performance compared to LSTMs in their original experiment and because the code was open source. However, other architectures might lead to different results. From the analysis presented above, we hypothesized that a process-based layer that includes a fast-flow channel might improve performance. Moreover, expanding the hybrid model's parameter range or the number of dynamic parameters might be beneficial. However, the added flexibility might come at the expense of model interpretability. Additionally, considering the fact that catchment-averaged precipitation values present a higher bias during ex-

treme events, strategies to overcome this limitation should be tested. Given the non-mass-conservative structure of the LSTM, systematic input biases can be accounted for. However, similar strategies should be evaluated for the hybrid case (e.g., considering a dynamic parameter that factorizes the precipitation input). Furthermore, other strategies to create a hybrid model, such as component replacement, should also be tested (Kraft et al., 2022; Höge et al., 2022). We encourage the hydrological community to expand the test cases presented here.

The training–test split applied in this study was intended as a form of stress-testing to get a sense of a model's capacity to generalize to unseen events. For the reasons stated in previous sections, this stress-testing method directly affects the saturation problem in the LSTM and the parameter optimization for the hybrid and conceptual models. In a practical case, one should not remove low-probability events from the training data. Furthermore, in an operational setting, all the data should be included during model training to increase the performance of the models (Nevo et al., 2022).

Lastly, differences between simulated and observed values, especially in extreme events, can also be attributed to higher uncertainty in the observed quantities, including discharge and precipitation (Di Baldassarre and Montanari, 2009; Westerberg and McMillan, 2015; Bárdossy and Anwar, 2023). We did not consider this type of uncertainty in our analysis as this would be outside of the scope of the paper.

## 4 Summary and conclusions

In this study, we evaluated the generalization capabilities of data-driven, hybrid, and conceptual models for predicting extreme hydrological events. Following the methodology proposed by Frame et al. (2022), we partitioned our data based on occurrence frequencies using the 5-year return period discharge as a threshold. We trained our models using information from water years with discharges strictly lower than the threshold and tested their performance on low-probability data. This setting was meant as a form of stress-test to get a sense of the model behavior with regard to extreme-streamflow events. Our findings indicated that the LSTM outperforms the hybrid and HBV models slightly for 1–5-year and 5–25-year return periods, and all models show similar performance for higher discharges.

The spatial analysis of the models' performance revealed that all three models exhibited higher errors in more arid basins, consistently with findings reported in the literature (Martinez and Gupta, 2010; Gauch et al., 2021; Newman et al., 2022). Regarding the differences between the models, the LSTM presented lower errors than the hybrid model in more arid basins, particularly for events in the 5–25-year and 25–50-year return period categories. This disparity can be attributed to the structural limitations of the HBV model,

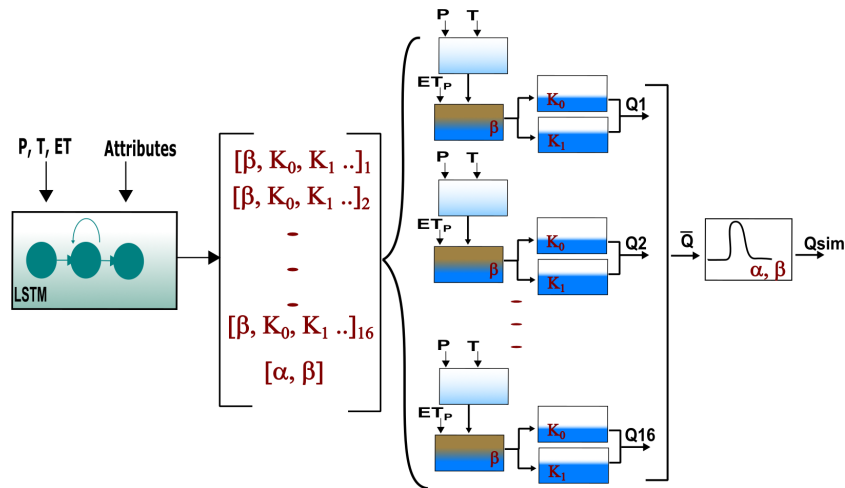
which assumes that discharge is a function of basin storage, a premise that may not align with runoff-generating processes in arid basins. Given that the hybrid model is regularized by an HBV layer, this structural deficiency would explain why the LSTM outperforms the hybrid model in this area. On the contrary, for the events of the return period of 100+ years, the hybrid model outperformed the LSTM in a cluster of basins located on the northwestern coast of the US. This behavior can be linked to the LSTM's theoretical discharge saturation limit, which is determined during training. In the northwestern cluster, the event's magnitude exceeded the saturation limit of the LSTM, preventing the LSTM from simulating the observed discharges. As discussed before, the training–test split used in this study artificially increased the saturation problem as it constricted the data space the model was fitted to. In practice, this problem can be attenuated by also considering low-probability events during training. Nevertheless, a theoretical limit will still exist, which is not a desirable property for a hydrological model. Additional research to overcome this limitation should be encouraged.

Expanding on the analysis to include the most extreme scenarios across the whole dataset, it can be concluded that all models underestimated the scenarios with the most extreme flow. However, the hybrid model and HBV were able to simulate higher discharges than the LSTM and presented an error distribution with longer tails toward smaller values. Upon further investigation, we noticed that the reasons for underestimating the extreme-flow scenarios were different. For the LSTM, its saturation limit was reached. On the other hand, the hybrid and HBV models underestimated the discharge due to structural deficiencies and possible bias in the input data. The dynamic parameterization of hybrid models might help reduce the former by changing the model response based on current conditions. This idea is conceptually similar to how an LSTM operates, with the gate structures operating based on current and past conditions.

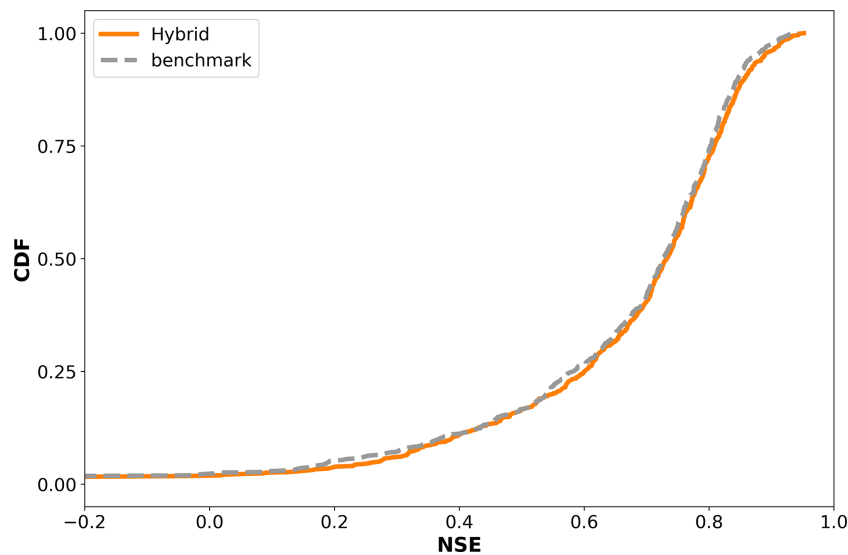
Overall, in most of the experiments performed here, we did not find strong evidence suggesting that there is a significant difference between the extrapolation capabilities of LSTM networks and hybrid models. However, hybrid models did report slightly lower errors in the most extreme cases and were able to produce higher peak discharges. We leave it to the reader's discretion to choose the model that best suits their needs.

Appendix A: Benchmarking hybrid model

For our hybrid model, we used the  $\delta_n(\gamma^t, \beta^t)$  architecture proposed by Feng et al. (2022). A scheme of this architecture is shown in Fig. A1. Given that our experiment pipeline was executed in the NeuralHydrology package, we first had to benchmark our model implementation against the original case. Figure A2 shows that our model implementation produced similar results to the one reported by Feng et al. (2022).



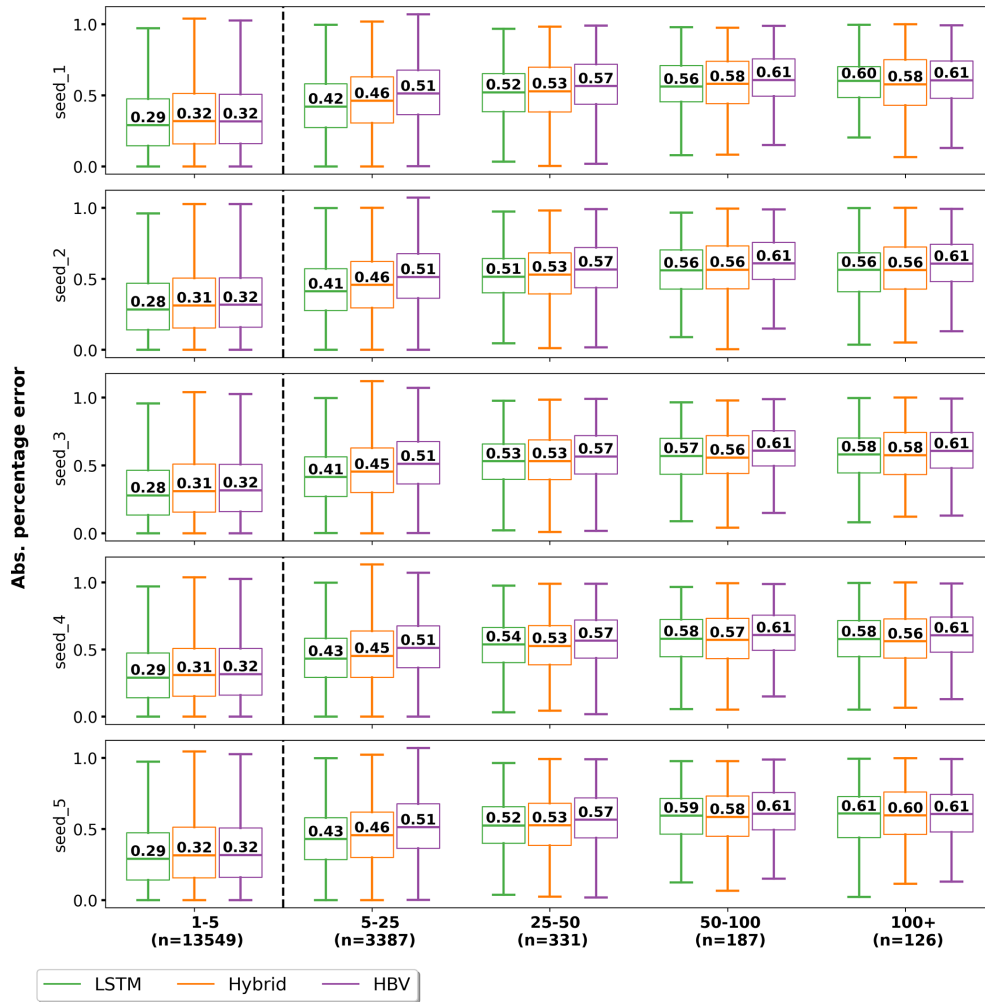
**Figure A1.** Scheme of the hybrid model structure. The LSTM predicts the parameters used to parameterize the different hydrological modules. In total, the LSTM produced 210 parameters (16 HBV members, each with 13 parameters and 2 routing parameters). The 16 hydrological models are run in parallel. The produced discharges are averaged, and the averaged signal is further routed using a unit hydrograph based on the gamma function. The output of the routing module is retrieved as the final simulated discharge.



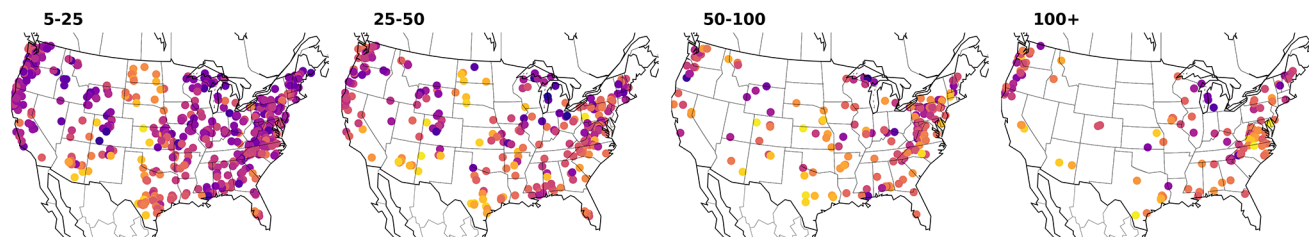
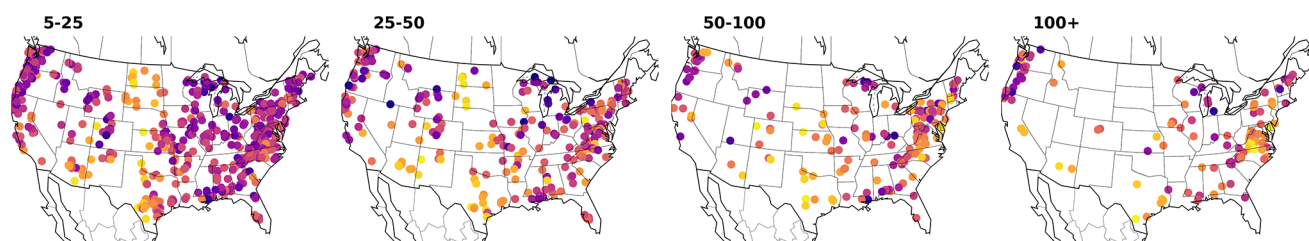
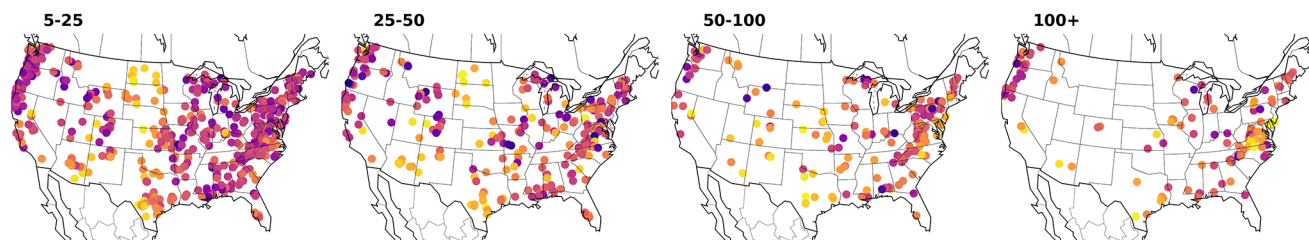
**Figure A2.** Cumulative density function (CDF) of the Nash–Sutcliffe efficiency (NSE) for different models, generated using 671 basins of the CAMELS-US dataset.

**Appendix B: Impact of random model initialization on absolute percentage error metric**

Figure B1 shows the effect of different model initializations on the APE metric. The ranking of the models in the last three categories (25–50 years, 50–100 years, 100+ years) varies depending on the model initialization. This indicates that the differences in the median values are within the statistical noise, and we cannot conclude that one model is better than the other.



**Figure B1.** Variation in absolute percentage error (APE) due to random initialization of the LSTM and hybrid models.

**Appendix C: Spatial visualization and comparison of model performance****(a) LSTM****(b) Hybrid****(c) HBV**

**Figure C1.** Spatial visualization of absolute percentage error (APE) for the different models and the different return periods. Each point is associated with one basin. The scale indicates the median APE between observed and simulated values for all the events associated with the respective basin and return period.

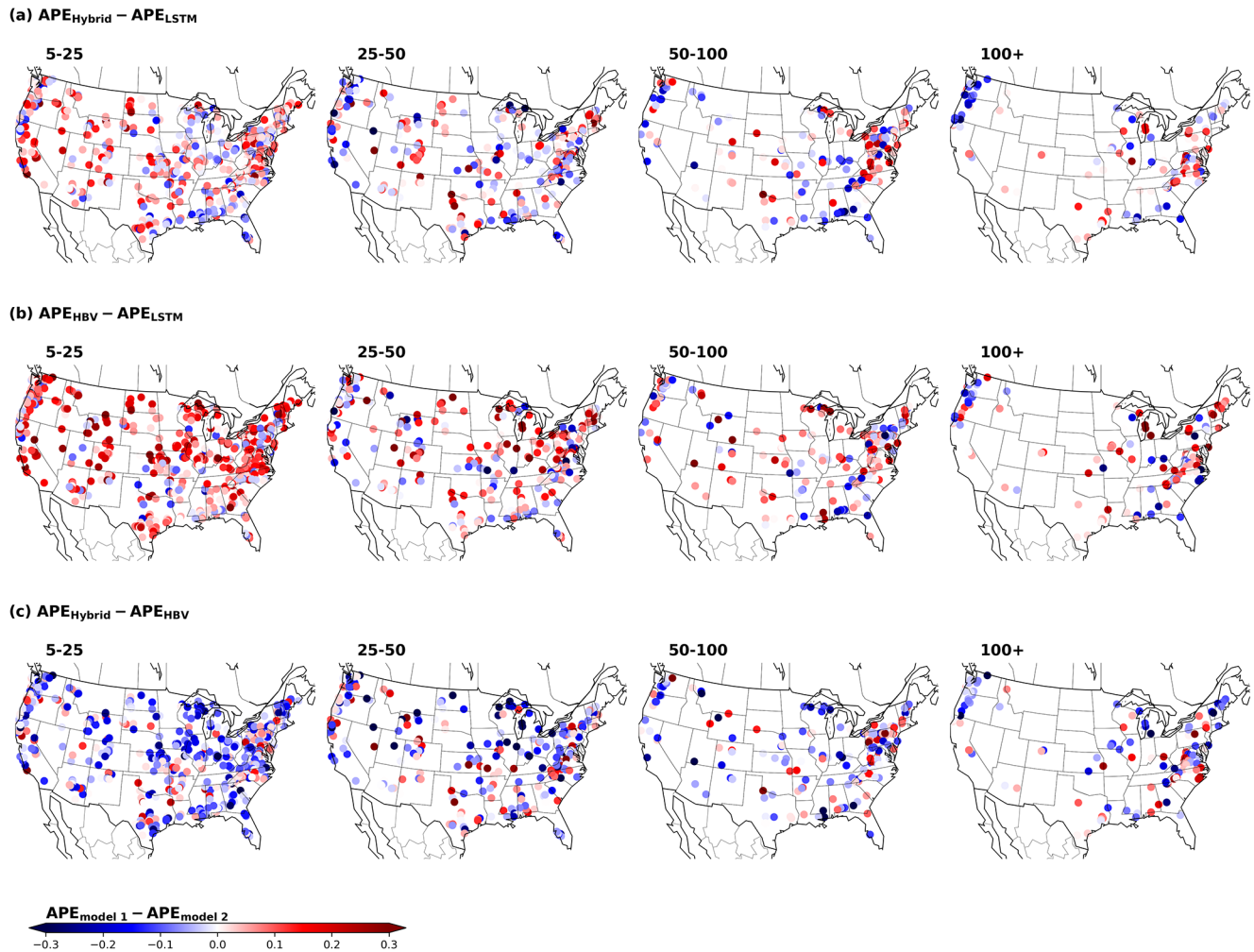


**Figure C2.** Spatial visualization of the difference between the absolute percentage error (APE) for the different models. Each point is associated with one basin. The scale indicates the difference between the median APE of the different models. The difference is calculated based on the order in which the models are named:  $APE_{\text{model 1}} - APE_{\text{model 2}}$ ; therefore, negative (blue) values indicate that model 1 performed better, while positive (red) values indicate that model 2 performed better.

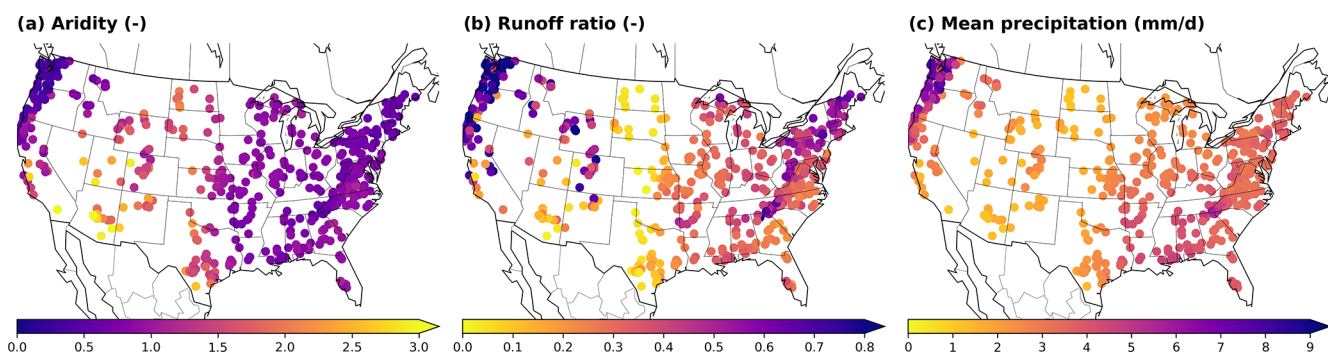


**Figure C3.** Spatial visualization of basin-averaged static attributes. Each point is associated with one basin. (a) Spatial variability of aridity. (b) Spatial variability of runoff ratio. (c) Spatial variability of mean daily precipitation.

#### Appendix D: Temporal variation in dynamic parameters

Figure D1 shows the temporal variation in the dynamic parameters of the hybrid model for three basins. For the first two basins, we can see clear cyclic patterns, in which the parameters are adjusted in dry or wet seasons to produce less or more water. These patterns were discussed in Acuña Espinoza et al. (2024) for experiments conducted in CAMELS-GB and suggest the possibility that the LSTM controls the HBV models in a consistent way. However, further investigation is needed to understand the LSTM–HBV interaction. In the third basin, the hydrograph does not present such a clear distinction between dry and wet seasons, and we can observe more variation in the parameters.

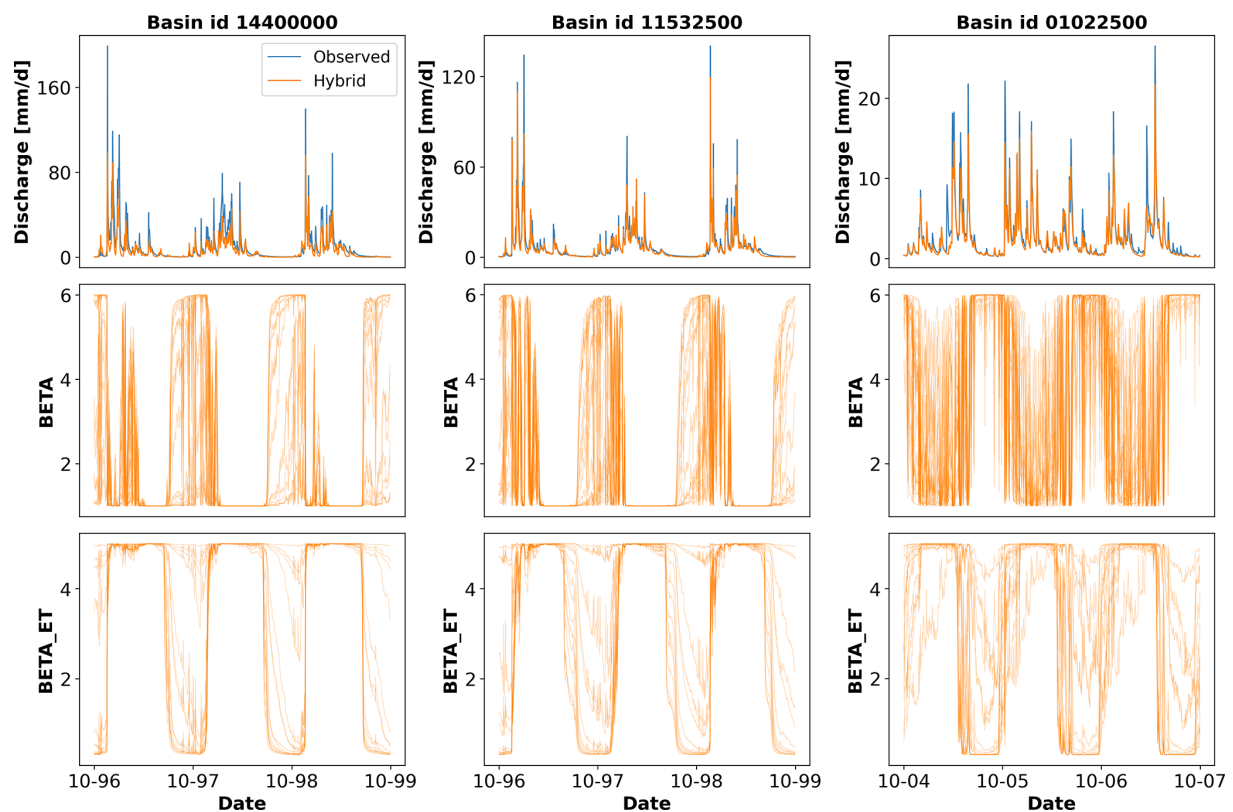


**Figure D1.** Time series indicating the variation in parameters for three different basins and their association with the simulated hydrographs.

*Code availability.* The code used to conduct all the analyses can be found at <https://doi.org/10.5281/zenodo.14191623> (Acuña Espinoza, 2024) and as part of our GitHub repository [https://github.com/eduardoAcunaEspinoza/hybrid\\_extrapolation/tree/v0.2](https://github.com/eduardoAcunaEspinoza/hybrid_extrapolation/tree/v0.2) (last access: 12 January 2025).

*Data availability.* The CAMELS-US dataset is freely available at <https://doi.org/10.5065/D6MW2F4D> (Newman et al., 2022). All the data generated for this publication can be found at <https://doi.org/10.5281/zenodo.14191623> (Acuña Espinoza, 2024).

*Author contributions.* The original idea of the paper was developed by all the authors. The codes were written by EAE, with support from FK, MG, and DK. The simulations were conducted by EAE. The results were further discussed by all the authors. The draft of the paper was prepared by EAE. Reviewing and editing was provided by all the authors. Funding was acquired by UE. All the authors have read and agreed to the current version of the paper.

*Competing interests.* At least one of the (co-)authors is a member of the editorial board of *Hydrology and Earth System Sciences*. The peer-review process was guided by an independent editor, and the authors also have no other competing interests to declare.

*Disclaimer.* Publisher's note: Copernicus Publications remains neutral with regard to jurisdictional claims made in the text, published maps, institutional affiliations, or any other geographical representation in this paper. While Copernicus Publications makes every effort to include appropriate place names, the final responsibility lies with the authors.

*Acknowledgements.* We would like to thank the referees, Basil Kraft and Shijie Jiang, as their input in the review process allowed us to produce a better paper. We would also like to thank the Google Cloud Program (GCP) team for awarding us credits to support our research and run the models. Uwe Ehret would like to thank the people of Baden-Württemberg who, through their taxes, provide the basis for this research.

*Financial support.* This project has received funding from the KIT Center for Mathematics in Sciences, Engineering and Economics under the seed funding program. Daniel Klotz acknowledges funding from the Helmholtz Initiative and Networking Fund (Young Investigator Group COMPOUNDX, grant agreement no. VH-NG-1537).

The article processing charges for this open-access publication were covered by the Karlsruhe Institute of Technology (KIT).

*Review statement.* This paper was edited by Manuela Irene Brunner and reviewed by Basil Kraft and Shijie Jiang.

## References

Acuña Espinoza, E.: Analyzing the generalization capabilities of hybrid hydrological models for extrapolation to extreme events, Zenodo [code and data set], <https://doi.org/10.5281/zenodo.14191623>, 2024.

Acuña Espinoza, E., Loritz, R., Álvarez Chaves, M., Bäuerle, N., and Ehret, U.: To bucket or not to bucket? Analyzing the performance and interpretability of hybrid hydrological models with

dynamic parameterization, *Hydrol. Earth Syst. Sci.*, 28, 2705–2719, <https://doi.org/10.5194/hess-28-2705-2024>, 2024.

Addor, N., Newman, A. J., Mizukami, N., and Clark, M. P.: The CAMELS data set: catchment attributes and meteorology for large-sample studies, *Hydrol. Earth Syst. Sci.*, 21, 5293–5313, <https://doi.org/10.5194/hess-21-5293-2017>, 2017.

Bárdossy, A. and Anwar, F.: Why do our rainfall–runoff models keep underestimating the peak flows?, *Hydrol. Earth Syst. Sci.*, 27, 1987–2000, <https://doi.org/10.5194/hess-27-1987-2023>, 2023.

Bergström, S.: THE HBV MODEL – its structure and applications, Tech. rep., Sveriges Meteorologiska Och Hydrologiska Institut, <https://www.smhi.se/en/publications/the-hbv-model-its-structure-and-applications-1.83591> (last access: 12 January 2025), 1992.

Di Baldassarre, G. and Montanari, A.: Uncertainty in river discharge observations: a quantitative analysis, *Hydrol. Earth Syst. Sci.*, 13, 913–921, <https://doi.org/10.5194/hess-13-913-2009>, 2009.

Donoho, D.: 50 years of data science, *J. Comput. Graph. Stat.*, 26, 745–766, <https://doi.org/10.1080/10618600.2017.1384734>, 2017.

Duan, Q., Sorooshian, S., and Gupta, V. K.: Optimal use of the SCE-UA global optimization method for calibrating watershed models, *J. Hydrol.*, 158, 265–284, [https://doi.org/10.1016/0022-1694\(94\)90057-4](https://doi.org/10.1016/0022-1694(94)90057-4), 1994.

Ehret, U., van Pruijssen, R., Bortoli, M., Loritz, R., Azmi, E., and Zehe, E.: Adaptive clustering: reducing the computational costs of distributed (hydrological) modelling by exploiting time-variable similarity among model elements, *Hydrol. Earth Syst. Sci.*, 24, 4389–4411, <https://doi.org/10.5194/hess-24-4389-2020>, 2020.

England Jr., J. F., Cohn, T. A., Faber, B. A., Stedinger, J. R., Thomas Jr., W. O., Veilleux, A. G., Kiang, J. E., and Mason Jr., R. R.: Guidelines for determining flood flow frequency – Bulletin 17C, Tech. rep., US Geological Survey, <https://doi.org/10.3133/tm4B5>, 2019.

Feng, D., Fang, K., and Shen, C.: Enhancing streamflow forecast and extracting insights using long-short term memory networks with data integration at continental scales, *Water Resour. Res.*, 56, e2019WR026793, <https://doi.org/10.1029/2019WR026793>, 2020.

Feng, D., Liu, J., Lawson, K., and Shen, C.: Differentiable, learnable, regionalized process-based models with multiphysical outputs can approach state-of-the-art hydrologic prediction accuracy, *Water Resour. Res.*, 58, e2022WR032404, <https://doi.org/10.1029/2022WR032404>, 2022.

Frame, J. M., Kratzert, F., Klotz, D., Gauch, M., Shalev, G., Gilon, O., Qualls, L. M., Gupta, H. V., and Nearing, G. S.: Deep learning rainfall–runoff predictions of extreme events, *Hydrol. Earth Syst. Sci.*, 26, 3377–3392, <https://doi.org/10.5194/hess-26-3377-2022>, 2022.

Gauch, M., Kratzert, F., Klotz, D., Nearing, G., Lin, J., and Hochreiter, S.: Rainfall–runoff prediction at multiple timescales with a single Long Short-Term Memory network, *Hydrol. Earth Syst. Sci.*, 25, 2045–2062, <https://doi.org/10.5194/hess-25-2045-2021>, 2021.

Hochreiter, S. and Schmidhuber, J.: Long short-term memory, *Neural Comput.*, 9, 1735–1780, <https://doi.org/10.1162/neco.1997.9.8.1735>, 1997.



- Höge, M., Scheidegger, A., Baity-Jesi, M., Albert, C., and Fenicia, F.: Improving hydrologic models for predictions and process understanding using neural ODEs, *Hydrol. Earth Syst. Sci.*, 26, 5085–5102, <https://doi.org/10.5194/hess-26-5085-2022>, 2022.
- Houska, T., Kraft, P., Chamorro-Chavez, A., and Breuer, L.: SPOTting model parameters using a ready-made python package, *PLoS One*, 10, e0145180, <https://doi.org/10.1371/journal.pone.0145180>, 2015.
- Jiang, S., Zheng, Y., and Solomatine, D.: Improving AI system awareness of geoscience knowledge: symbiotic integration of physical approaches and deep learning, *Geophys. Res. Lett.*, 47, e2020GL088229, <https://doi.org/10.1029/2020GL088229>, 2020.
- Kingma, D. P and Ba, J.: Adam: A method for stochastic optimization, arXiv [preprint], <https://doi.org/10.48550/arXiv.1412.6980>, 2014.
- Kraft, B., Jung, M., Körner, M., Koirala, S., and Reichstein, M.: Towards hybrid modeling of the global hydrological cycle, *Hydrol. Earth Syst. Sci.*, 26, 1579–1614, <https://doi.org/10.5194/hess-26-1579-2022>, 2022.
- Kratzert, F., Klotz, D., Shalev, G., Klambauer, G., Hochreiter, S., and Nearing, G.: Towards learning universal, regional, and local hydrological behaviors via machine learning applied to large-sample datasets, *Hydrol. Earth Syst. Sci.*, 23, 5089–5110, <https://doi.org/10.5194/hess-23-5089-2019>, 2019.
- Kratzert, F., Gauch, M., Nearing, G., and Klotz, D.: Neural-Hydrology — A Python library for Deep Learning research in hydrology, *Journal of Open Source Software*, 7, 4050, <https://doi.org/10.21105/joss.04050>, 2022.
- Kratzert, F., Gauch, M., Klotz, D., and Nearing, G.: HESS Opinions: Never train a Long Short-Term Memory (LSTM) network on a single basin, *Hydrol. Earth Syst. Sci.*, 28, 4187–4201, <https://doi.org/10.5194/hess-28-4187-2024>, 2024.
- Lees, T., Buechel, M., Anderson, B., Slater, L., Reece, S., Coxon, G., and Dadson, S. J.: Benchmarking data-driven rainfall-runoff models in Great Britain: a comparison of long short-term memory (LSTM)-based models with four lumped conceptual models, *Hydrol. Earth Syst. Sci.*, 25, 5517–5534, <https://doi.org/10.5194/hess-25-5517-2021>, 2021.
- Loritz, R., Dolich, A., Acuña Espinoza, E., Ebeling, P., Guse, B., Götze, J., Hassler, S. K., Hauffe, C., Heidebüchel, I., Kiesel, J., Mälicke, M., Müller-Thomy, H., Stölzle, M., and Tarasova, L.: CAMELS-DE: hydro-meteorological time series and attributes for 1582 catchments in Germany, *Earth Syst. Sci. Data*, 16, 5625–5642, <https://doi.org/10.5194/essd-16-5625-2024>, 2024.
- Martinez, G. F. and Gupta, H. V.: Toward improved identification of hydrological models: A diagnostic evaluation of the “abcd” monthly water balance model for the conterminous United States, *Water Resour. Res.*, 46, W08507, <https://doi.org/10.1029/2009WR008294>, 2010.
- Nash, J. E. and Sutcliffe, J. V.: River flow forecasting through conceptual models part I – a discussion of principles, *J. Hydrol.*, 10, 282–290, [https://doi.org/10.1016/0022-1694\(70\)90255-6](https://doi.org/10.1016/0022-1694(70)90255-6), 1970.
- Nearing, G. S., Kratzert, F., Sampson, A. K., Pelissier, C. S., Klotz, D., Frame, J. M., Prieto, C., and Gupta, H. V.: What role does hydrological science play in the age of machine learning?, *Water Resour. Res.*, 57, e2020WR028091, <https://doi.org/10.1029/2020WR028091>, 2021.
- Nevo, S., Morin, E., Gerzi Rosenthal, A., Metzger, A., Barshai, C., Weitzner, D., Voloshin, D., Kratzert, F., Elidan, G., Dror, G., Begelman, G., Nearing, G., Shalev, G., Noga, H., Shavitt, I., Yuklea, L., Royz, M., Giladi, N., Peled Levi, N., Reich, O., Gilon, O., Maor, R., Timnat, S., Shechter, T., Anisimov, V., Gigi, Y., Levin, Y., Moshe, Z., Ben-Haim, Z., Hassidim, A., and Matias, Y.: Flood forecasting with machine learning models in an operational framework, *Hydrol. Earth Syst. Sci.*, 26, 4013–4032, <https://doi.org/10.5194/hess-26-4013-2022>, 2022.
- Newman, A., Sampson, K., Clark, M., Bock, A., Viger, R. J., Blodgett, D., Addor, N., and Mizukami, M.: CAMELS: Catchment Attributes and MEteorology for Large-sample Studies, Version 1.2, UCAR/NCAR [data set], <https://doi.org/10.5065/D6MW2F4D>, 2022.
- Newman, A. J., Clark, M. P., Sampson, K., Wood, A., Hay, L. E., Bock, A., Viger, R. J., Blodgett, D., Brekke, L., Arnold, J. R., Hopson, T., and Duan, Q.: Development of a large-sample watershed-scale hydrometeorological data set for the contiguous USA: data set characteristics and assessment of regional variability in hydrologic model performance, *Hydrol. Earth Syst. Sci.*, 19, 209–223, <https://doi.org/10.5194/hess-19-209-2015>, 2015.
- Reichstein, M., Camps-Valls, G., Stevens, B., Jung, M., Denzler, J., and Carvalhais, N.: Deep learning and process understanding for data-driven Earth system science, *Nature*, 566, 195–204, <https://doi.org/10.1038/s41586-019-0912-1>, 2019.
- Shen, C., Laloy, E., Elshorbagy, A., Albert, A., Bales, J., Chang, F.-J., Ganguly, S., Hsu, K.-L., Kifer, D., Fang, Z., Fang, K., Li, D., Li, X., and Tsai, W.-P.: HESS Opinions: Incubating deep-learning-powered hydrologic science advances as a community, *Hydrol. Earth Syst. Sci.*, 22, 5639–5656, <https://doi.org/10.5194/hess-22-5639-2018>, 2018.
- Shen, C., Appling, A. P., Gentine, P., Bandai, T., Gupta, H., Tartakovsky, A., Baity-Jesi, M., Fenicia, F., Kifer, D., Li, L., Liu, X., Ren, W., Zheng, Y., Harman, C. J., Clark, M., Farthing, M., Feng, D., Kumar, P., Aboelyazeed, D., Rahmani, F., Song, Y., Beck, H. E., Bindas, T., Dwivedi, D., Fang, K., Höge, M., Rackauckas, C., Mohanty, B., Roy, T., Xu, C., and Lawson, K.: Differentiable modelling to unify machine learning and physical models for geosciences, *Nature Reviews Earth and Environment*, 4, 552–567, <https://doi.org/10.1038/s43017-023-00450-9>, 2023.
- Slater, L. J., Arnal, L., Boucher, M.-A., Chang, A. Y.-Y., Moulds, S., Murphy, C., Nearing, G., Shalev, G., Shen, C., Speight, L., Villarini, G., Wilby, R. L., Wood, A., and Zappa, M.: Hybrid forecasting: blending climate predictions with AI models, *Hydrol. Earth Syst. Sci.*, 27, 1865–1889, <https://doi.org/10.5194/hess-27-1865-2023>, 2023.
- Tsai, W.-P., Feng, D., Pan, M., Beck, H., Lawson, K., Yang, Y., Liu, J., and Shen, C.: From calibration to parameter learning: harnessing the scaling effects of big data in geoscientific modeling, *Nat. Commun.*, 12, 5988, <https://doi.org/10.1038/s41467-021-26107-z>, 2021.
- US Geological Survey: National Water Information System data available on the World Wide Web (USGS Water Data for the Nation), <https://doi.org/10.5066/F7P55KJN>, 2016.
- Virtanen, P., Gommers, R., Oliphant, T. E., Haberland, M., Reddy, T., Cournapeau, D., Burovski, E., Peterson, P., Weckesser, W., Bright, J., van der Walt, S. J., Brett, M., Wilson, J., Millman, K. J., Mayorov, N., Nelson, A. R. J., Jones, E., Kern, R., Larson, E., Carey, C. J., Polat, I., Feng, Y., Moore, E. W., VanderPlas, J., Laxalde, D., Perktold, J., Cimrman, R., Henriksen, I., Quintero, E. A., Har-

- ris, C. R., Archibald, A. M., Ribeiro, A. H., Pedregosa, F., van Mulbregt, P., Vijaykumar, A., Bardelli, A. P., Rothberg, A., Hilboll, A., Kloeckner, A., Scopatz, A., Lee, A., Rokem, A., Woods, C. N., Fulton, C., Masson, C., Häggström, C., Fitzgerald, C., Nicholson, D. A., Hagen, D. R., Pasechnik, D. V., Olivetti, E., Martin, E., Wieser, E., Silva, F., Lenders, F., Wilhelm, F., Young, G., Price, G. A., Ingold, G.-L., Allen, G. E., Lee, G. R., Audren, H., Probst, I., Dietrich, J. P., Silterra, J., Webber, J. T., Slavič, J., Nothman, J., Buchner, J., Kulick, J., Schönberger, J. L., de Miranda Cardoso, J. V., Reimer, J., Harrington, J., Rodríguez, J. L. C., Nunez-Iglesias, J., Kuczynski, J., Tritz, K., Thoma, M., Newville, M., Kümmerer, M., Bolingbroke, M., Tartre, M., Pak, M., Smith, N. J., Nowaczyk, N., Shebanov, N., Pavlyk, O., Brodtkorb, P. A., Lee, P., McGibbon, R. T., Feldbauer, R., Lewis, S., Tygier, S., Sievert, S., Vigna, S., Peterson, S., More, S., Pudlik, T., Oshima, T., Pingel, T. J., Robitaille, T. P., Spura, T., Jones, T. R., Cera, T., Leslie, T., Zito, T., Krauss, T., Upadhyay, U., Halchenko, Y. O., and Vázquez-Baeza, Y.: SciPy 1.0: fundamental algorithms for scientific computing in Python, *Nat. Methods*, 17, 261–272, <https://doi.org/10.1038/s41592-019-0686-2>, 2020.
- Vrugt, J. A.: Markov chain Monte Carlo simulation using the DREAM software package: theory, concepts, and MATLAB implementation, *Environ. Modell. Softw.*, 75, 273–316, <https://doi.org/10.1016/j.envsoft.2015.08.013>, 2016.
- Westerberg, I. K. and McMillan, H. K.: Uncertainty in hydrological signatures, *Hydrol. Earth Syst. Sci.*, 19, 3951–3968, <https://doi.org/10.5194/hess-19-3951-2015>, 2015.